Coastal Dynamics 2017
Paper No. 201

RIP CURRENTS AT WAVE-AVERAGED TIME SCALES VIA RADAR REMOTE SENSING

Annika O'Dea[1] and Merrick C. Haller[2]

Abstract

Rip currents, seaward-directed currents flowing through the surf zone and beyond, are an important component of nearshore circulation systems. In this study, X-band radar images of rip currents from Duck, NC, along with accompanying wind and wave measurements, are used to assess the forcing mechanisms controlling the offshore obliquity of rip currents relative to the shoreline. The relevant parameters in the alongshore momentum balance are assessed at the locations of three current sensors in the domain, and the associated radar images are used to determine how these different forcing mechanisms influence the obliquity of the rip current in and out of the surf zone. Results suggest that the direction of rip obliquity outside of the surf zone is primarily driven by the alongshore wind stress, although additional analyses are necessary to address simplifications made in the analysis. Preliminary observations of large rip currents from Newport, OR, are presented along with a discussion of future research areas focusing on the parameters influencing the obliquity and cross-shore extent of these large-scale rip systems.

Key words: remote sensing, microwave radar, rip currents, nearshore hydrodynamics, nearshore momentum balances

1. Introduction

Rip currents are narrow offshore-oriented currents, generated in the surf zone, that flow through the breaker line and extend offshore. They are frequent features on many beaches all over the world, and play an important role in the exchange of waters, nutrients, sediment, and organisms between the surf zone and inner shelf. Rip currents also pose a serious danger to ocean swimmers, and are the leading cause of lifeguard rescues on public beaches (Fletemeyer and Leatherman, 2010).

Because of their importance in nearshore zones and their status as a major public safety hazard, significant efforts have been made to improve our understanding of the factors influencing the formation, strength, and morphology of rip currents as well as our ability to accurately model and forecast rips. A number of field studies have been conducting using nearshore pressure and current meter arrays to collect information on rip currents (e.g. Sonu, 1972; Guza and Thornton, 1989; Aagaard et al., 1997; Brander 1999; MacMahan et al., 2005). However, the transient nature of many rips and the need for dense spatial and temporal measurements make capturing and evaluating rip currents using these methods a difficult and expensive task. Lagrangian techniques such as drifters have provided a more synoptic picture of rip current circulation (Schmidt et al., 2003; Johnson and Pattiaratchi, 2004; MacMahan et al., 2010), but are still limited in their capacity to provide long-term observations over large areas.

The application of remote sensing techniques to nearshore areas has expanded the type of data we can collect relating to rip currents as well as the temporal and spatial scales over which these data can be collected. Optical assessments of rip current location and persistence over long time scales (i.e. several years) have been conducted using video techniques (Holman et al., 2006). However, this technique is based on the identification of rip-associated morphological features (primarily rip channels in alongshore bars), and therefore is limited in the amount of information it can provide about the flow field itself. A few other studies have employed Doppler sonar (Smith and Largier, 1995; Vagle et al., 2001), airborne infrared imagery (Marmorino et al., 2013), and synthetic aperture radar (SAR) (da Silva et al., 2006; da Silva, 2008) to identify rip currents or rip-associated hydrodynamic features, but to date these methods have only been applied to a limited number of rip current events.

Preliminary observations from shore-based microwave radar suggest that these instruments could

[1]School of Civil and Construction Engineering, Oregon State University, USA. odeaa@oregonstate.edu
[2]School of Civil and Construction Engineering, Oregon State University, USA. merrick.haller@oregonstate.edu

provide a valuable additional source of rip current data. Takewaka and Yamawaka (2010) presented time-averaged radar intensity images with cross-shore oriented bright features that were confirmed as rip currents using GPS-equipped floaters. Haller et al. (2014) also presented time-averaged radar intensity images that showed a regular sequence of tidally-recurring rip currents that were verified using a cross shore array of current meters, and against a numerical model (Wilson et al., 2014). Although non-Doppler marine radars (like those used in the two studies described above) do not have the capability of directly estimating rip current velocities, these studies have shown that radar images can provide important information about the physical and temporal characteristics of rip current systems over large spatial scales.

Although microwaves only penetrate seawater to a depth of millimeters or centimeters, past studies have shown that many hydrodynamic features have a recognizable surface signature that can be identified in microwave radar images (e.g. Alpers, 1985; Lyzenga, 1991). In general, it has been established that surface current gradients can lead to changes in surface roughness (and potentially short-scale wave breaking in some cases) due to interactions between short surface waves and the underlying current field, which result in distinct regions of increased or decreased radar backscatter in radar images (Lyzenga, 1998; Kudryavtsev, 2005; Plant et al. 2010). These images therefore provide useful information about the underlying current field, and can be used to address questions related to the frequency, evolution, and spatial extent of rip current systems. When coupled with wind and wave measurements, they can also be used to assess forcing mechanisms controlling different aspects of rip current morphology. Finally, the high spatial and temporal resolution of the instrument, large footprint, and capacity for long-term deployment suggest that these instruments could be used in the development of real-time rip current identification and monitoring systems.

Observations from X-band radar imagery presented in Haller et al. (2014) showed a consistent rip current system occurring nearly every low tide during an 11-day period at the USACE Field Research Facility in Duck, NC. At certain times, the rip current was shown to extend several surf zone widths offshore, significantly farther than the expected extent of rip current flow suggested by past studies (Dalrymple et al., 2011; Castelle et al., 2014). Additionally, many of these rip currents extended away from the shore at an oblique angle. In this study, the same marine radar data set is further analyzed to assess the forcing mechanisms controlling the obliquity of the rip currents observed offshore. Analyses of the components of the alongshore momentum balance are used to evaluate the relative importance of different forcing mechanisms contributing to this alongshore flow at different cross-shore locations. Preliminary observations from a rip current system on the US west coast (Newport, OR) are also presented that show rip current flow extending up to two kilometers offshore. Areas for future work are discussed that focus on assessing the forcing mechanisms controlling rip obliquity and the cross-shore extent of flow in these large rip systems.

2. Field site 1: Duck, NC

2.1. *Observations of rip current obliquity*

Radar images were collected at the US Army Corps of Engineers (USACE) Field Research Facility (FRF) in Duck, NC (on the east coast of the US) from September 7-17, 2010, as part of a pilot experiment for the Data Assimilation and Remote Sensing for Littoral Applications (DARLA) project funded by the Office of Naval Research (Jessup et al., 2012). The radar was installed on a 10 m tower in the northern part of the FRF property (x = 17.4 m, y = 971.4 m, and antenna elevation = 13.8 m in the FRF coordinate system). The FRF coordinate system has the positive x- axis pointing offshore, the y-axis pointing 18° west of True North, with the North American Vertical Datum of 1988 (NAVD88) used as the vertical datum. The radar collects an image of the ocean surface every 1.25 s (0.80 Hz imaging frequency). Additional details on the radar system can be found in Haller et al. (2014) and Catalán et al. (2011).

Throughout the data collection period, the radar collected hourly sets of 640 images over approximately 15 minute periods beginning at the start of each hour. The uncalibrated intensity values were then averaged at each location over the 15 minute period, resulting in a 15 minute time-averaged intensity image. This process removes individual wave crests from the images, but allows for the identification of areas of persistent high or low backscatter. All images were mapped into the FRF coordinate system.

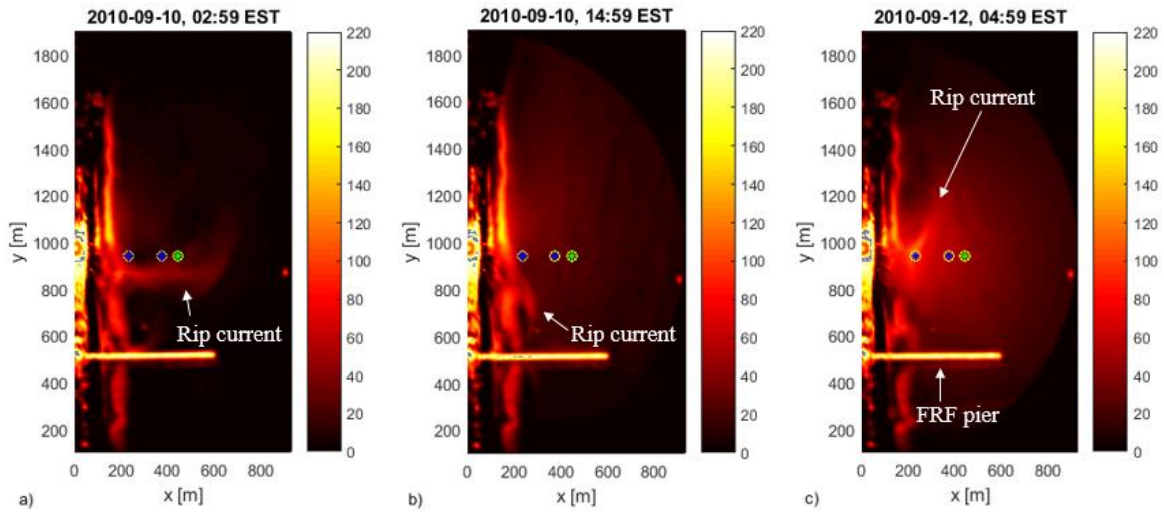

Figure 1. Examples of 15 minute time-averaged X-band radar intensity images from the FRF, showing a) a relatively shore-normal rip current, b) a southern-oriented rip, and c) a northern-oriented rip. The locations of the Aquadopps used in the analysis are shown in blue, and the location of the AWAC is shown in green.

Breaking waves result in enhanced backscatter in radar imagery. The time-averaged radar images from the data collection period show a bright streak parallel to the shoreline, which indicates where waves were actively breaking during the 15 minute data collection period. This bright streak generally extends to around x = 200 m at low tide, which is the approximate location of a shore parallel sandbar (Figure 1, Figure 3). Outside of the surf zone, rip currents are seen as cross-shore oriented features of enhanced backscatter centered near y = 900 m. Radar imaged rip currents were evident during nearly every low tide that occurred during the data collection period. The frequency and stable location of the rip currents indicate a morphologic rip forcing mechanism.

The radar images showed that, in many cases, the rip currents extended away from the shoreline at an oblique angle (referred to in this paper as the rip current obliquity). Rip currents were observed with both southern- and northern-oriented obliquity (Figure 1b and 1c, respectively). Many of the rips with southern-oriented obliquity appeared to be part of a recirculating system that extended to around x = 300 m and then moved back onshore (Figure 1b). A number of the rip currents appeared to extend significantly farther offshore, at times extending to x = 700 m or beyond (Figure 1a).

In situ current measurements from an array of continuously-deployed hydrodynamic instruments maintained by the FRF were used to confirm the presence of rip currents. The array included two Nortek Aquadopps and one acoustic wave and current profiler (Nortek AWAC) (Mulligan et al., 2011). The Aquadopps were located at (x,y,z) = (233, 940, -3.3 m) and (375, 939, -4.3 m) (referred to as adop1 and adop2, respectively) and the AWAC was located at (x,y,z) = (466, 938, -5.0 m) (Figure 1). At the end of each hour, the instruments recorded vertical profiles of bidirectional currents in three 5-minute bursts, with a sampling rate of 1 Hz. The vertical profiles were averaged over the 5-minute burst, and then vertically averaged to provide depth- and time-averaged currents at 35, 45, and 55 minutes past the hour for each sensor. For consistency, the sensor measurements were interpolated to the center of the radar sampling interval (7 minutes past the hour).

The measured alongshore velocity v and cross-shore velocity u from the three current sensors (adop1, adop2, and AWAC) are shown in Figure 2a and 2b, respectively. The alongshore current velocities measured at the two most offshore locations (adop2, x = 375 m and AWAC, x = 446 m) were very similar throughout the data collection period. The alongshore velocity measured closer to the shoreline (adop1, x = 233 m) followed similar trends to the velocities measured at the other sites, but was slightly more variable. Greater differences were seen in the cross-shore velocities measured at the three sensors. The sensor located closest to the shoreline (adop1) showed a regular, offshore directed spike in cross-shore velocity, with magnitudes ranging from 10 to over 30 cm/s. These cross-shore flows correspond with low tide periods. The outer two sensors show visible spikes in cross-shore velocity centered on 2010-09-10 00:00 EST and 2010-09-14 06:00 EST. Outside of these two time periods, the more offshore-located

sensors did not measure cross-shore velocities greater than 10 cm/s. The differences in alongshore and cross-shore velocities at adop1 versus adop2 and AWAC suggest that there were different forcing mechanisms influencing the flow at adop1.

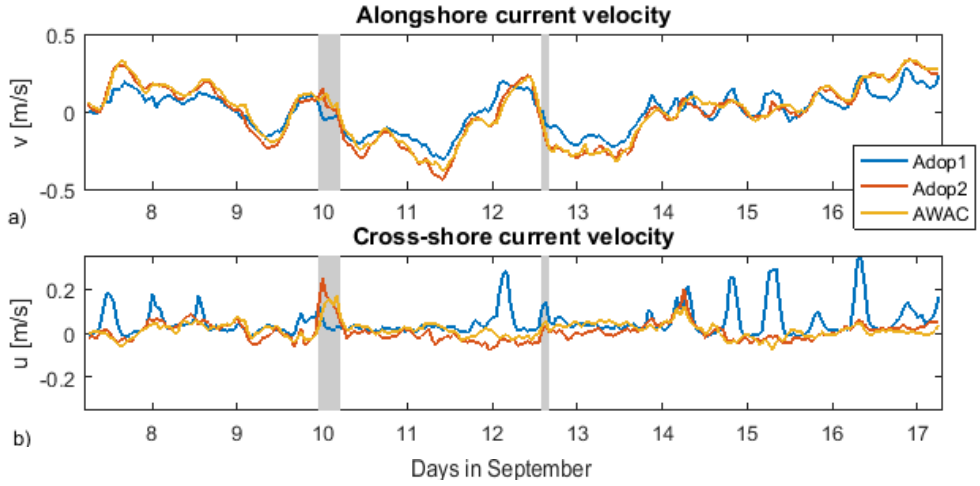

Figure 2. a) Alongshore velocity and b) cross-shore velocity from the sensors deployed during the radar data collection period. The grey bands indicate the events analyzed in the subsequent discussion and figures.

Bathymetric surveys were conducted on 2010 09-06 and 2010 09-15 using two amphibious vehicles owned and operated by the FRF. The surveys show a single alongshore bar located between x = 150 m and 200 m which was stable for the duration of the data collection period. A gap in the bar was present at y = 750 – 1000 m, with the depth in the gap around 1 m greater than at the bar crest (Haller et al., 2014). The measured bathymetry along with a cross-shore profile from the earlier survey at y = 700 m are shown in Figure 3.

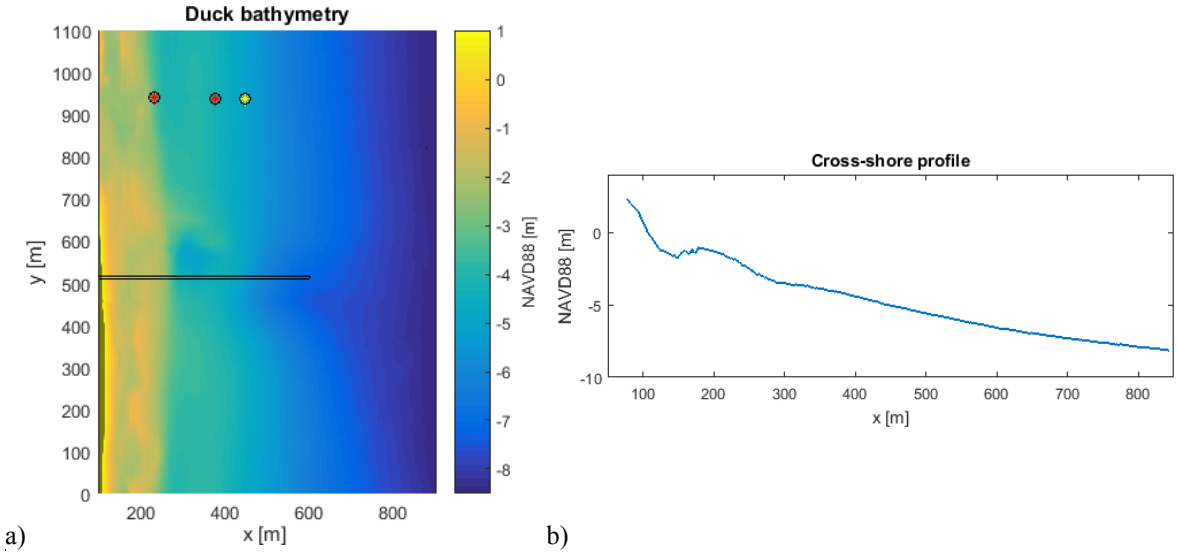

Figure 3. a) Measured bathymetry at Duck from the 2010 09-06 survey. The symbols indicate the locations of the two Aquadopps (red) and the AWAC (yellow), and the black line at y = 515 m shows the location of the FRF pier; b) cross-shore profile at y = 700 m.

2.2. *Drivers of rip current obliquity*

To determine the factors contributing to the observed rip current obliquity, the forcing parameters in the alongshore momentum balance were assessed at different cross-shore locations. Assuming Coriolis acceleration is negligible, the one-dimensional, depth-averaged alongshore momentum equation in the nearshore region reduces to a balance between wind and wave forcing, alongshore pressure gradients, bottom stress, and mixing, which can be written as:

$$-\frac{1}{\rho}\frac{dS_{yx}}{dx}+\frac{\tau_y^w}{\rho}-gh\frac{d\zeta}{dy}=\frac{\tau_y^b}{\rho}-\frac{d}{dx}\left(\nu h\frac{d\bar{v}}{dx}\right) \tag{1}$$

where S_{yx} is the off-diagonal component of the radiation stress tensor, τ_y^w is the alongshore wind stress, h is the water depth, ρ is the density of water, $d\zeta/dy$ is the tidally-induced alongshore slope of the mean sea surface (10-100 km scale), τ_y^b is the mean alongshore bottom stress, and ν is the depth-averaged eddy viscosity (Ruessink et al. 2001; Lentz et al. 1999). In the surf zone, the primary contributions to this balance are the forcing by obliquely incident breaking waves (in the form of the radiation stress gradients) and bottom stress, with additional components including alongshore pressure gradients, cross-shelf mixing processes, and alongshore wind stress (Lentz et al., 1999). In the inner shelf, defined by Lentz et al. (1999) as the region from edge of the surf zone to the 13 m isobaths, the alongshore momentum balance is primarily between surface (wind) and bottom stresses, although alongshelf pressure gradients can be important in some settings (Lentz et al., 1999).

Wind stress, wave-induced radiation stress gradients, and bottom stress were assessed at the location of the three sensors for the duration the data collection period. The wave-induced forcing in the nearshore is a result of the cross-shore gradient in the radiation stress S_{xy}. Assuming the wave field is narrow in frequency and directional space, the radiation stress can be written as:

$$S_{xy}=\frac{1}{8}\rho g H_{rms}^2\frac{c_g}{c}\cos\theta_m\sin\theta_m+2E_r\cos\theta_m\sin\theta_m \tag{2}$$

which includes both a wave and roller contribution on the right hand side of the equation. In order to calculate the radiation stress gradients at the location of the sensors, the incident wave conditions obtained from a two-dimensional array of bottom-mounted pressure sensors located at the 8 m water depth contour (x = ~915 m) (Long, 1996) were propagated across the domain using a 1-D wave model, following Ruessink et al. (2001), which assumes limited alongshore variability in the wave field or bathymetry. The wave model included two coupled differential equations describing the wave and roller energy balances averaged over time. Assuming that wave field is narrow-banded in frequency and directional space, the wave energy balance can be written as

$$\frac{d}{dx}\left(\frac{1}{8}\rho g H_{rms}^2 c_g\cos\theta_m\right)=-D_{br}-D_{bf} \tag{3}$$

where x is the cross-shore coordinate, g is the acceleration of gravity, H_{rms} is the root-mean-square wave height, c_g is the group velocity, θ_m is the mean wave angle, D_{br} is dissipation due to breaking waves, and D_{bf} is the dissipation due to bottom friction (Ruessink et al., 2001). The roller energy balance rollers is given by:

$$\frac{d}{dx}\left(2E_r c\cos\theta_m\right)=-D_r+D_{br} \tag{4}$$

(Stive and De Vriend, 1994), where E_r is the roller energy density, c is the phase speed, and D_r is the roller dissipation, written as

$$D_r=\frac{2gE_r\sin\beta}{c} \tag{5}$$

where β is the wave-front slope (Duncan, 1981, Deigaard, 1993). A value of 0.1 was used for β, following Ruessink et al. (2001). The bottom friction term was modeled following Nielson (1983), and the breaking wave dissipation term was modeled following Battjes and Stive (1985), using standard parameters given in the texts for all constants. The cross-shore depth profile was taken from the measured bathymetry (y = 700 m, 2010 09-06 survey), the measured tide level at the FRF, and the calculated setup (following Battjes and Janssen, 1978). The measured bathymetric transect did not extend out to the 8 m array, so the transect was extended to x = 915 m assuming a 1:100 slope. The measured values of H_{rms}, peak wave period T_p, and mean wave direction θ_m from the 8 m array were used as input conditions in the wave model, which then solved for H_{rms} and D_r across the transect using a forward stepping scheme. Combining equations (2), (3), and (4) and assuming that $D_{bf} << D_{br}$ in the surf zone, the gradient in S_{xy} can be written as

$$\frac{dS_{yx}}{dx} = -\frac{\sin\theta_m}{c} D_r \tag{6}$$

following Ruessink et al., (2001). The gradient in S_{xy} was determined using this formulation at the location of each of the sensors for each hour of the data collection period.

Although the local wave-induced alongshore forcing is a function of the cross-shore gradients in S_{xy}, the total S_{xy} outside of the surf zone can be seen as measure of the total wave-induced alongshore forcing across the surf zone for beaches with limited alongshore variability. The radiation stress S_{xy} was calculated using equation (2) with the measured wave conditions at the 8 m array to determine the direction and magnitude of wave-induced forcing in the surf zone for each hour in the data collection period.

Wind measurements were obtained at 19.4 m above mean sea level using an RM Young marine anemometer deployed and maintained as part of the normal FRF operations, located at the end of the FRF pier. Wind speed and direction were found by vector averaging the data (sampled at 1 Hz) over sampling periods of 10 minutes. Alongshore wind stress was calculated using measured wind speed and direction following Smith (1988). Bottom stress was estimated using a linear drag law ($\tau^{by} = \rho r v_b$) using r = 5 x 10^{-4} m/s and measured alongshore current velocities (following Lentz et al., 1999).

Measurements of the alongshelf pressure gradients due to the tidally-induced alongshore slope of the water surface were not available for the analysis period. However, past studies at Duck have shown that this term is significantly smaller than the wind or wave forcing (Ruessink et al., 2001). In this study, the alongshore pressure gradient was assumed negligible.

In addition to the forcing parameters, the offshore edge of the surf zone was located for each hour using two different surf zone definitions, to determine whether the sensors were located inside or out of the surf zone. The edge of the surf zone was defined by Castelle et al. (2014) as the location where the roller energy E_r exceeded 10% of its cross-shore maximum, and more simply by Lentz et al. (1999) as the location where H_{sig}/h = 0.33. The edge of the surf zone was found using both definitions and the locations were compared.

2.3. *Analysis*

Plots of the significant wave height H_{sig}, peak period T_p (both measured at the 8 m array), the off-diagonal radiation stress component S_{xy} (calculated from measured wave conditions at the 8 m array), and the tidal elevation are shown in Figure 4. Measured H_{sig} ranged from 0.25 m to 1.14 m during the data collection period, with peak periods ranging from 3.5 s to 15.6 s.

The location of the edge of the surf zone was found for each time point throughout the data collection period. The size of the surf zone was influenced primarily by significant wave height and tidal elevation. Using the Castelle et al. (2014) definition, the outer edge of the surf zone ranged from x = 109 m to x = 243 m. Using the Lentz et al. (1999) definition, the surf zone extended farther offshore, from x = 116 m to x = 287 m. The surf zone extended significantly farther offshore during low tides, as increased wave-breaking occurred over the bar (located near x = 190 m, shown in Figure 3). The calculated locations of the offshore extent of the surf zone are shown in Figure 5.

Comparing the calculated extent of the surf zone with the locations of the sensors, it was determined that only adop1 was located in the surf zone at any point during the data collection period. With both surf zone

definitions, the AWAC was located at least 150 m outside of the surf zone at all times during the data collection period. This suggests that forcing from radiation stress gradients at the location of the AWAC was little to none, and wind stress was the primary driver of the alongshore flow at this location during this time period.

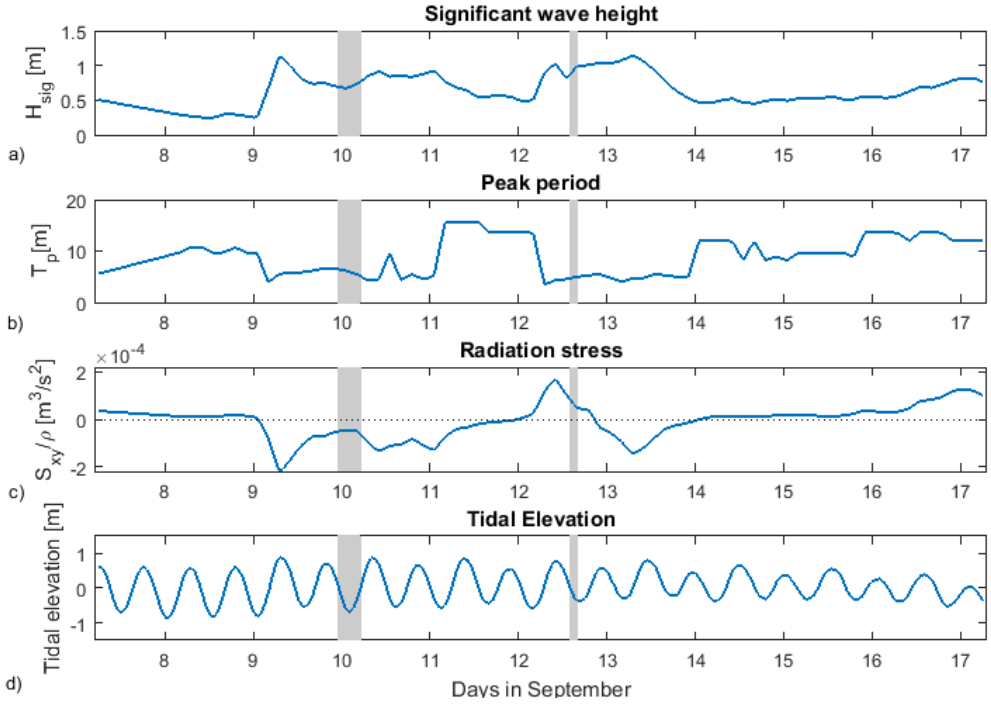

Figure 4. a) Significant wave height H_{sig}, b) peak period T_p, c) calculated radiation stress S_{xy} and d) tidal elevation during the radar data collection period. The grey bands indicate the events analyzed in the subsequent discussion and figures.

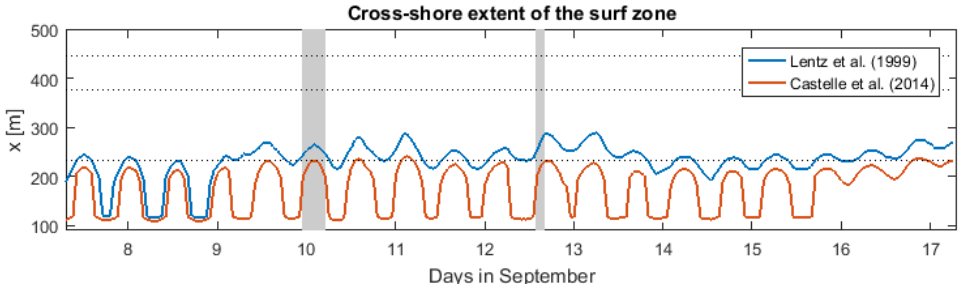

Figure 5. The cross-shore extent of the surf zone calculated using the Lentz et al. (1999) definition (in blue) and the Castelle et al. (2014) definition (in red). The dotted horizontal lines show the locations of adop1 (x = 233m), adop2 (x = 375 m) and AWAC (x = 446 m). The grey bands indicate the events analyzed in the subsequent discussion and figures.

To further assess this, the wind stress and radiation stress gradients at the location of adop1 and AWAC were plotted along with the bottom stress calculated using the measured current velocities (Figure 6). As expected, the radiation stress gradients at the location of adop1 are only nonzero at a few times during the data collection period (09-09 12:00-15:00; 09-10 00:00-04:00; 09-10 12:00-16:00; 09-11 01:00-05:00; 09-12 05:00; 09-12 15:00-19:00; 09-13 04:00-07:00; and 09-16 18:00 to 09-17 01:00 EST), which correspond to the periods where the sensor was located in or near the surf zone (shown in Figure 5). The radiation stress gradients were zero at the location of the AWAC for the entire data collection period. The bottom stress and wind stress appear to follow very similar trends, and were found to have a correlation coefficient of 0.76 at AWAC and 0.74 at adop1. To further distinguish between these forcing mechanisms, two periods

in which the wind- and wave-induced forces were opposing one another during a measured flow reversal period captured in radar imagery were identified, which will be referred to as Events 1 and 2 (grey bands in Figure 4-6). Radar images of Events 1 and 2 were assessed to determine the obliquity of the rip current at these periods, and whether this obliquity appears to relate primarily to the wind or wave forcing.

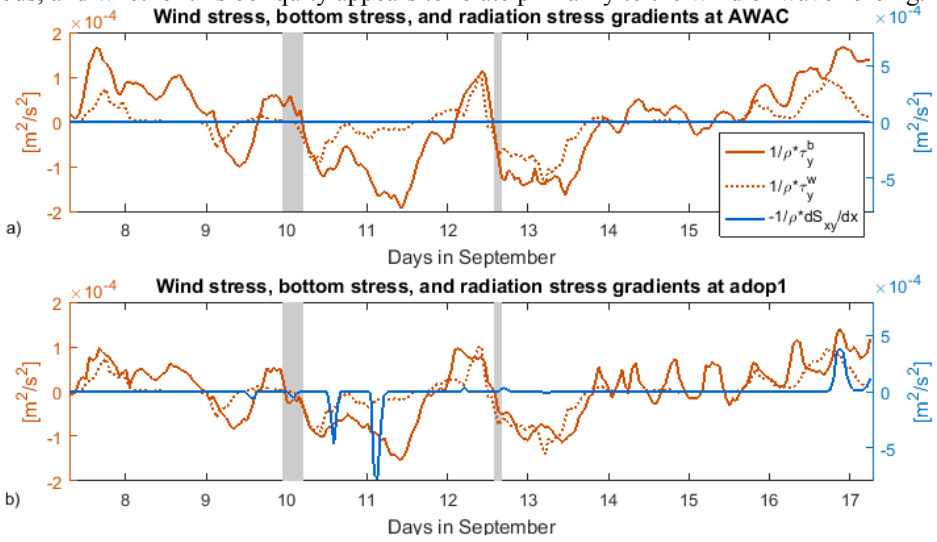

Figure 6. Alongshore bottom stress τ_y^b/ρ and wind stress τ_y^w/ρ (both in red), and radiation stress gradients $1/\rho\ dS_{xy}/dx$ (blue) at the location of a) AWAC and b) adop1. The grey bands indicate the Events 1 and 2.

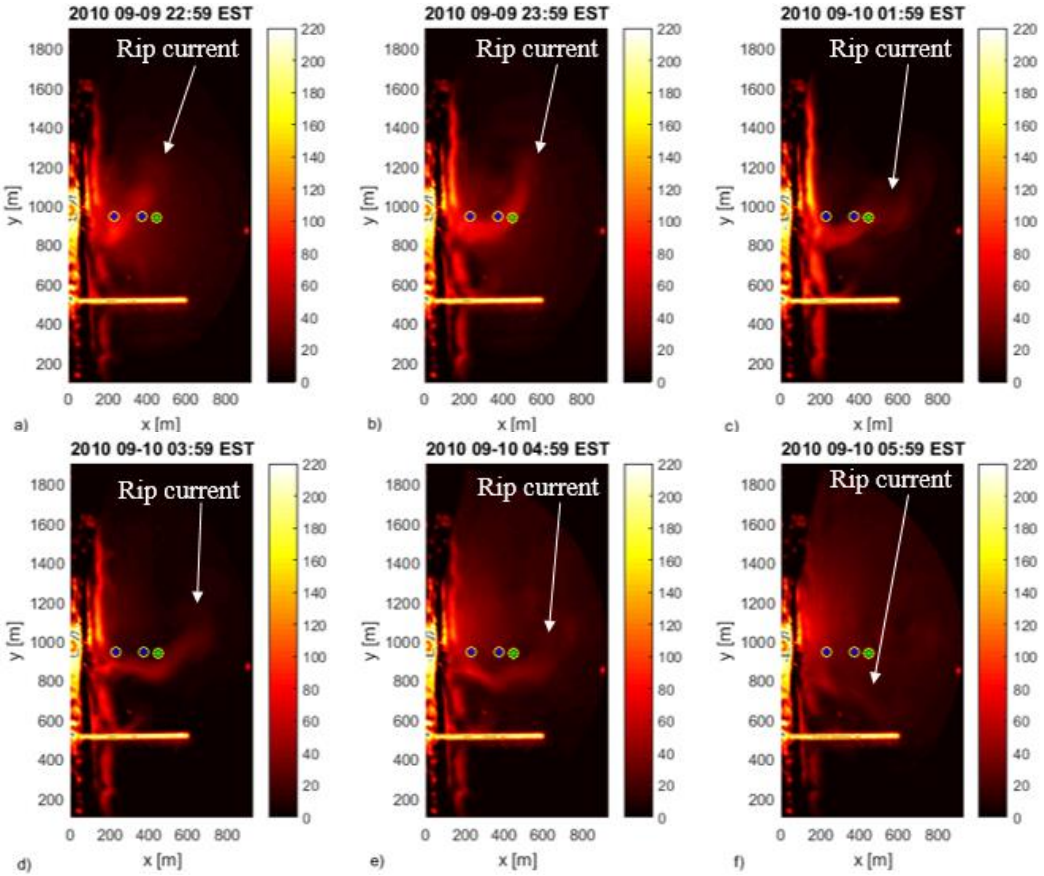

Figure 7. Radar images from 2010-09-09 22:59 EST to 05:59 EST (Event 1), which correspond to the first grey band shown in Figures 4-6, 8. The measured alongshore velocity at the location of the AWAC (x = 446 m) moves from positive (toward the north) to negative during this event.

During Event 1 (from 2010 09-09 22:59 EST to 2010 09-10 05:59 EST), the wind stress is positive in the hours leading up to this event, and remains slightly positive until 2010-09-10 02:07 EST (the middle of the event). The radiation stress gradients are zero at the location of adop1 in the hours leading up to the event, and become negative during the event. Radar images from this event show a reversal in the orientation of the rip current during the event (Figure 7). In the images, it appears that the base of the rip current changes orientation before the more offshore portions of the rip. The time series of current measurements shown in Figure 2 confirm this observation. The velocity measured at adop1 becomes negative starting at 2010-09-10 00:07 EST, but the velocity measured by the AWAC does not reverse direction until five hours later.

Further analysis of this time period shows that the reversal in the current direction measured by adop1 corresponds to the increase in wave-induced forcing at this location as the tide drops and the sensor moves close to (or into) the surf zone (Figure 8). At this point, it appears that the alongshore flow at the location of adop1 is being forced primarily by the wave-induced radiation stress gradients (and is therefore negative), but the current at the location of the AWAC is primarily being forced by the wind stress (and is therefore positive). Only after the wind stress becomes negative does the offshore flow reverse direction (Figure 8). In this case, the rip current orientation at the base appears to be controlled by the wave-induced forcing, but offshore of adop1 the rip obliquity is being forced by wind stress.

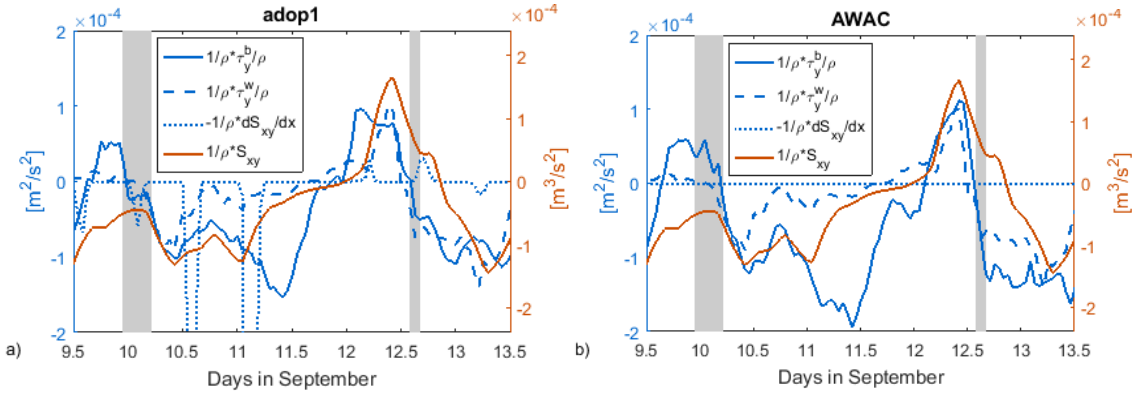

Figure 8. Alongshore bottom stress τ_y^b/ρ and wind stress τ_y^w/ρ, wave-induced radiation stress gradients $1/\rho\ dS_{xy}/dx$ (all in blue) and the radiation stress S_{xy}/ρ (red) at the location of a) adop1 and b) AWAC.

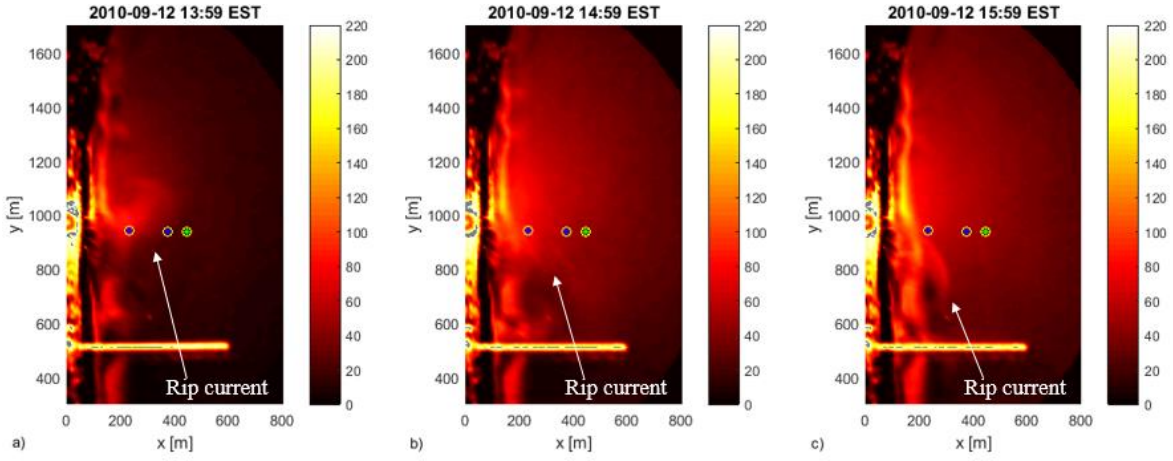

Figure 9. Radar images from 2010-09-12 13:59 EST to 15:59 EST (Event 3) at hourly intervals, which correspond to the second grey band shown in Figure 4-6, 8. The measured alongshore velocity at the location of the AWAC (x = 446 m) moves from positive (toward the north) to negative during this period.

The radar images from Event 2 (2010 09-12 13:59 EST to 2010 09-12 15:59 EST), shown in Figure 9, show a reversal in the orientation of the rip current (from the north to the south) and the formation of a

circulation cell. Similar to the earlier case, the flow reversal seen in the AWAC velocity data is also seen in the change in rip current orientation. The radiation stress calculated at the 8 m array was plotted in addition to the radiation stress gradients to determine the direction of the wave-induced forcing in the surf zone at times when the radiations stress gradients at the locations of the sensors were zero (Figure 8). The radiation stress is positive prior to and during this event, which would indicate that the forcing in the surf zone is positive (opposing the wind stress during the event). The current velocities measured at both sensors follow the direction of the wind stress for this period, again suggesting that the currents at these locations, and thus the obliquity of the rip current, is being forced primarily by the wind stress.

In these events, the obliquity of the rip currents appear to better agree with the direction of the wind forcing than the wave-induced forcing at the location of the AWAC. Without current meters inside the surf zone, however, we were unable to confirm that the current within the surf zone followed the calculated wave forcing as we have assumed (and thus validate our simplified calculations). Simplifications in this analysis included neglecting alongshore pressure gradients, Coriolis acceleration, and alongshore variability in the wave field and bathymetry, and it is possible that these factors were not negligible during this time. Additional analysis would be required to determine the role of these factors in influencing rip obliquity.

3. Field site 2: Newport, OR

3.1 *Future work: Offshore rip current extent*

A similar radar system was installed on a ~10 m tower located near the base of the south jetty at the mouth of the Yaquina River, a jetty-stabilized inlet in Newport, on the central Oregon coast. A rocky reef is located approximately 1-1.5 kilometers offshore, running roughly parallel to the shoreline from the tip of the north jetty to Yaquina Head, a headland located north of Newport. An inner bar is located inside of the reef (closer to the shoreline). Example radar images from Newport are shown in Figure 10, showing the location of the reef and jetties relative to the device.

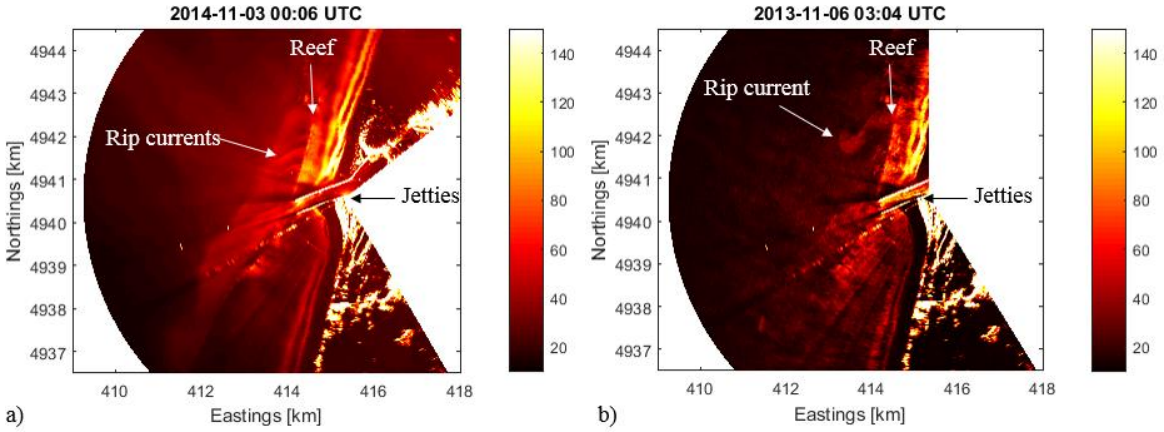

Figure 10. Examples of a 45-minute average (left) and a 2-minute average (right) radar intensity image from Newport, OR. The location of the reef is highlighted, along with the rip currents extending beyond the reef.

Preliminary radar observations from Newport show that at low tide, significant breaking can occur over the outer reef, generating morphologically-driven rip currents that extend out through a break in the reef (Figure 10). The cross-shore extent of this rip current reaches 2 km in some cases, almost triple the extent of the rip currents seen in Duck. Although past studies have shown that large-scale, morphologically-driven rip currents can occur in some environments (Brander and Short, 2000; Long and Özkan-Haller, 2005), the spatial extent of this rip is significantly larger than previously described rip current systems. Future work will focus on analyzing the parameters controlling the cross-shore extent of rip currents in these two different environments, as well as assessing the rip obliquity at this second site.

4. Conclusions

In this study, a series of radar observations from Duck, NC were analyzed to assess the forcing mechanisms controlling rip current obliquity at different cross-shore locations inside and out of the surf zone. The radar images were collected during an 11-day pilot experiment conducted at the USACE FRF in September 2010. Images showed a series of rip currents occurring nearly every low tide at approximately the same location throughout the data collection period, which often extended away from the shore at an oblique angle. Analysis of the wind stress, wave-induce radiation stress gradients, and bottom stress calculated at the locations of three sensors in the domain suggest that the obliquity of the rip current primarily agrees with the direction of wind forcing, which highlights the importance of including wind stress in nearshore circulation models. Additional analyses would be necessary to validate the simplifications made in the assessment and to analyze the role of additional forcing parameters neglected in this study.

Preliminary observations from radar images from Newport, OR were presented that show a large-scale rip current extending from the surf zone through a break in an offshore reef (located around ~ 1 km offshore) and beyond. Future work will include assessing the parameters influencing the offshore obliquity and cross-shore extent of this rip current system, and to determine how this compares with the cross-shore extent of rip flow observed in radar images from Duck.

Acknowledgements

The authors would like to acknowledge the staff at the Field Research Facility, Field Data Collections and Analysis Branch, US Army Corps of Engineers for providing the in situ data and for their support during field activities. Also, David Honegger and Patricio Catalán, for their significant efforts in the original data processing. Funding for the present analysis was provided by the Office of Naval Research (ONR) Award No. N00014-15-1-2020, with additional support from the School of Civil and Construction Engineering at Oregon State University.

References

Aagaard, T., Greenwood, B., and Nielsen, J. (1997). Mean currents and sediment transport in a rip channel. *Mar Geol, 140*(1-2), 25–45.

Alpers, W. (1985). Theory of radar imaging of internal waves. *Nature*, *314*(6008), 245–247.

Battjes, J.A. and Janssen, J.P.F.M. (1978). Energy loss and set-up due to breaking of random waves. *Proc 16th ICCE.* Pp 570-587, American Society of Civil Engineers, New York.

Battjes, J. A, and Stive, M. J. F. (1985). Calibration and verification of a dissipation model for random breaking waves. *J Geophys Res, 90*(C5), 9159–9167.

Brander, R.W. 1999. Field observations on the morphodynamic evolution of low wave energy rip current system. *Mar Geol*, 157: 199-217.

Brander, R.W. and Short, A.D. (2000). Morphodynamics of a large-scale rip current system at Muriwai Beach, New Zealand. *Mar Geol*, 165: 27-39.

Castelle, B., Reniers, A., and MacMahan, J. (2014). Bathymetric control of surf zone retention on a rip-channelled beach. *Ocean Dynam* 64:1221-1231.

Catalán, P.A., Haller, M.C., and Plant, W.J. (2011). Microwave backscattering from surf zone waves. *J Geophys Res: Oceans*, 3098–3120

Dalrymple, R.A., MacMahan, J.H., Reniers, A.J.H.M., and Nelko, V. (2011). Rip currents. *Annu Rev of Fluid Mech,* 43, 551-581.

da Silva, J. C. B. (2008). SAR observation of rip currents off the Portuguese coast. *Remote Sensing of the European Seas*, 399–410

da Silva, J., Sancho, F., and Quaresma, L. (2006). Observation of rip currents by synthetic aperture radar. *Proc SEASAR*, 23–26.

Deigaard, R. 1993. A note on the three dimensional shear stress distribution in the surf zone. *Coast Eng, 20,* 157-171.

Duncan, J.H. 1981. An empirical investigation of breaking waves produced by a towed hydrofoil, *Proc. R. Soc. Lonon, Ser A, 377,* 331-348.

Feddersen, F., Guza, R.T., Elgar, S., Herbers, T.H.C. (2000) Velocity moments in alongshore bottom stress parameterizations, *J Geophys Res*, 105: 8673-8686.

Fletemeyer, J. and Leatherman, S.2010. Rip current and beach safety education. *J Coastal Res,* 26(1):1-3.

Guza, R.T., and Thornton, E.B. 1989. Measuring surf zone dynamics: A. General measurements. In *Nearshore Sediment Transport,* ed. R.J. Seymour, 51-60. New York: Plenum.

Haller, M.C., Honegger, D., and Catalán, P.A. (2014). Rip Current Observations via Marine Radar, *J Waterw Port C - ASCE*, 140 (2), 115–124.

Holman, R. A., Symonds, G., Thornton, E. B., and Ranasinghe, R. (2006). Rip spacing and persistence on an embayed beach. *J Geophys Res: Oceans*, *111*(1), 1–17.

Jessup, A., et al. 2012. DARLA: Data assimilation and remote sensing for littoral applications. *Proc 2012 Fall Meeting*, American Geophysical Union, Washington DC Abstract OS14A-01.

Johnson, D., and Pattiaratchi, C. (2004). Transient rip currents and nearshore circulation on a swell-dominated beach. *J Geophys Res*, *109*(C02026).

Kudryavtsev, V. (2005). On radar imaging of current features: 1. Model and comparison with observations. *J Geophys Res*, *110*(C7), 1–27.

Lentz, S.L., Guza, R.T., Elgar, S., Feddersen, F., and Herbers, T.H.C. (1999) Momentum balances on the North Carolina Shelf. *J Geophys Res*, 104 (C8): 18205-18226.

Long, C.E. 1996. Index and bulk parameters for frequency-direction spectra measured at the CERC Field Research Facility, June 1994 to August 1995. Miscellaneous Paper CERC-96-6, U.S. Army Engineer Waterways Experiment Station, Vicksburg, MS.

Long, J.W. and Özkan-Haller, H.T. (2005). Offshore controls on nearshore rip currents. *J Geophys Res*, 110(C12007).

Lyzenga, D. R. (1991). Interaction of Short Surface and Electromagnetic Waves with Ocean Fronts. *J Geophys Res*, *96*(N6), 10,765–10,772.

Lyzenga, D. R. (1998). Effects of intermediate-scale waves on radar signatures of ocean fronts and internal waves. *J Geophys Res*, *103*(C9), 18,759–18,768.

MacMahan, J. H., Thornton, E. B., Stanton, T. P., and Reniers, A. J. H. M. (2005). RIPEX: Observations of a rip current system. *Mar Geol*, *218*(1-4), 113–134. https://doi.org/10.1016/j.margeo.2005.03.019

MacMahan, J., Brown, J., Brown, J., Thornton, E., Reniers, A., Stanton, T., and Senechal, N. (2010). Mean Lagrangian flow behavior on an open coast rip-channeled beach: A new perspective. *Mar Geol*, *268*(1-4), 1–15.

Marmorino, G.O., Smith, G. B., and Miller, W. D. (2013). Infrared remote sensing of surf-zone eddies. *IEEE J-STARS*, *6*(3), 1710–1718.

Mulligan, R.P., Hanson, J.L, and Hathaway, K.K. 2011. Observations of wave breaking and surf zone width from a real-time cross-shore array of wave and current sensors at Duck, N.C. *Proc IEEE/OES/CWTM 10th Current, Waves, and Turbulence Measurements (CWTM),* J. Rizoli White and A.J.Williams, 3rd eds, IEEE, Piscataway, NJ, 130-137

Nielson, P. 1983. Analytical determination of nearshore wave height due to refraction, shoaling and friction, *Coast Eng, 7*, 233-251.

Plant, W. J., Keller, W. C., Hayes, K., and Chatham, G. (2010). Normalized radar cross section of the sea for backscatter 2: Modulation by internal waves. *J Geophys Res*, *115*(C9), C09033.

Ruessink, B.G., Miles, J.R., Feddersen, F., Guza, R.T., and Elgar, S. 2001. Modeling the alongshore current on barred beaches. *J Geophys Res*, 106 (C10): 22451-22463.

Schmidt, W.E., Woodward, B. T., Millikan, K. S., Guza, R. T., Raubenheimer, B., and Elgar, S. (2003). A GPS-tracked surf zone drifter. *J Atmos Ocean Tech*, *20*(7), 1069–1075.

Smith, S. (1988). Coefficients for sea surface wind stress, heat flux, and wind profiles as a function of wind speed and temperature. *J Geophys Res*, 93 (C12): 15467-15472.

Smith, J.A., and Largier, J. L. (1995). Observations of nearshore circulation: Rip currents. *J Geophys Res*, *100*(C6), 10967.

Sonu, C.J. 1972. Field observation of nearshore circulation and meandering currents. *J Geophys Res*, 77(18): 3232-3247.

Stive, M.J.F. and De Vriend, H.J. 1994. Shear stress and mean flow in shoaling and breaking waves, in *Proc 24th ICCE*, pp. 594-608, American Society of Civil Engineers, New York.

Takewaka, S., and Yamakawa, T. (2008). Rip current observations with X-band radar. In *International Conference on Coastal Engineering* (pp. 2008–2011). Shanghai, China: International Engineering Research Council.

Vagle, S., Farmer, D. M., and Deane, G. B. (2001). Bubble transport in rip currents. *J Geophys Res*, *106*(C6), 11677.

Wilson, G.W., Özkan-Haller, H.T., Holman, R.A., Haller, M.C., Honegger, D.A., and Chickadel, C.C. (2014). Surf zone bathymetry and circulation predictions via data assimilation of remote sensing observations. *J Geophys Res Oceans*, 119: 1993-2016.